コンクリート工学年次論文集，Vol.45，No.2，2023

- Technical Paper -

IDENTIFICATION OF POTENTIAL FEATURES FOR CLASSIFYING SEISMIC DEFORMATION MODE FOR BUILDINGS WITHOUT SENSORS ON SOME FLOORS

Trevor Z. YEOW [*1] and Koichi KUSUNOKI [*2]

ABSTRACT

Building deformation mode identification, which is important for evaluating safety in structural health monitoring applications following seismic events, may be difficult to perform if there are some floors without sensors. This study proposed potential features based on the response of monitored floors which may indicate the correct deformation mode. These features were evaluated against shake-table test data of steel frames and numerical analyses of RC frame buildings. The features were found to be reasonable and can be used in machine-learning applications to identify deformation modes.

Keywords: Deformation mode, structural health monitoring, earthquake, safety limit, machine learning

1. INTRODUCTION

Structural health monitoring is an increasingly popular tool for rapidly and accurately evaluating building safety after an earthquake. This requires monitoring the response of buildings using various equipment (e.g., accelerometers, GPS, video cameras).

Methods exist to use floor acceleration and/or displacement data to derive a capacity curve [1] which can then be used to evaluate the building damage level [2]. Fig. 1 shows an example, where the "representative" response is the floor response condensed to an equivalent single-degree-of-freedom response. Kusunoki [2] proposed defining the boundary between the "moderate" and "severe" damage state as the maximum response permitted during a 1st seismic event to ensure that the safety limit is not exceeded in a 2nd seismic event of the same intensity.

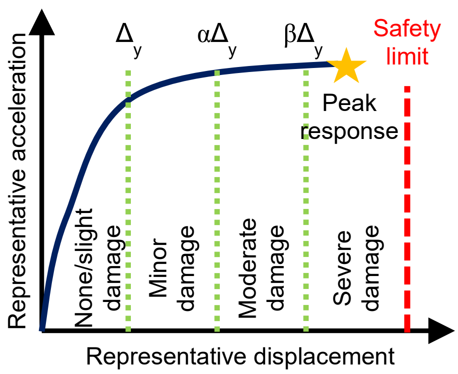

Fig. 1 Use of representative capacity curve for damage evaluation

A limitation of current methods is that sensors are often not placed on every floor due to cost, space, or usage restrictions. As such, the exact deformation mode (e.g., sidesway or soft-story) is not obvious. An example is shown in Fig. 2, where two deformation modes may be possible from the same observation.

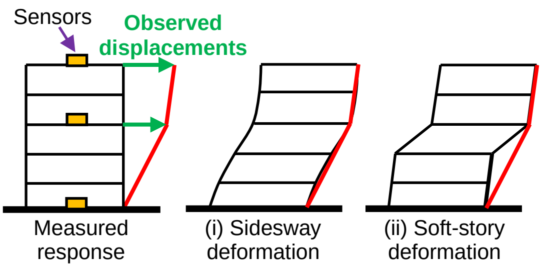

Fig. 2 Example of different deformation modes for same known displacements

The need to correctly identify the deformation mode is important for two reasons. Firstly, if the response of non-instrumented floors was estimated via interpolation, the representative response may be underpredicted for soft-story cases [3]. Secondly, the safety limit itself will differ depending on the deformation type. To demonstrate the latter, consider Fig. 3. Assuming the same allowable interstory drift ratio limit (θ_p) for both cases, and that the roof displacements are similar at yielding, the sidesway case will incur greater displacements at the roof level under the same drift limit, resulting in a greater safety limit.

This study looks to identify various features which can be used in machine-learning applications for classifying the deformation mode. First, various features based on theoretical concepts were proposed. Then, these features were evaluated against data from an experimental test of small-scale steel frames and numerical analyses of reinforced concrete (RC) frames. It should be noted that this paper will only focus on the

*1 Project Researcher, Earthquake Research Institute, University of Tokyo, JCI Member
*2 Professor, Earthquake Research Institute, University of Tokyo, JCI Member

identification of potential features, while the machine learning application is outside the scope of this paper. Furthermore, only displacement-based features were considered as they are likely to correlate better with soft-story failure (e.g., inelastic displacements will concentrate on the critical floor) compared to other building response measures (e.g., accelerations).

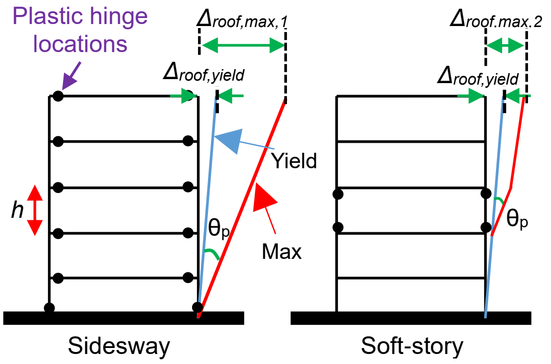

Fig. 3 Difference in roof displacements at safety limit condition

2. IDENTIFICATION OF POTENTIAL FEATURES

2.1 Concentration of inelastic response

One feature which could be used to identify soft-story failure could be based on the concentration of inelastic response. Consider the scenario shown in Fig. 4. If the inelastic displacement (δ_{in}) at the roof level, which is the difference between the maximum recorded displacement (δ_{max}) and the yield displacement (δ_y), is similar to that of the 3rd floor, then it is very likely that soft-story failure had occurred below the 3rd floor.

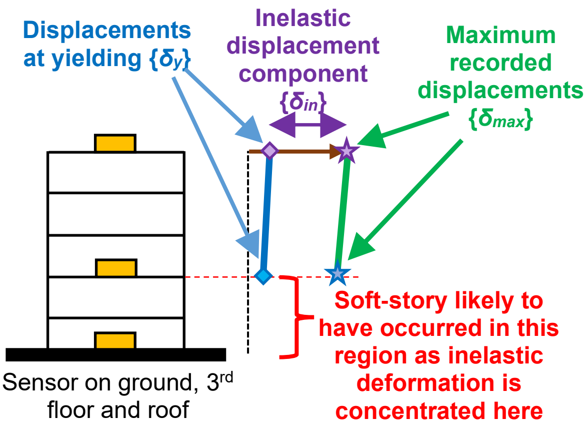

Fig. 4 Illustration of yield, inelastic and maximum recorded displacements

To evaluate if inelastic deformation is concentrated within a certain region of the building, one could compare the increase in inelastic displacements between adjacent sensors against the total inelastic displacement at the roof. The calculation of this feature, $R_{1,i}$ is shown in Eq. (1), where the i subscript denotes each region between sensors starting from the bottom of the structure (e.g., i = 1 is the region between the ground and 3rd floor sensors, and i = 2 is the region between the 3rd floor and roof sensors in Fig. 4), and the L and U subscripts denote the lower and upper sensors within the i^{th} region, respectively. As $R_{1,i}$ approaches 1.0, this would indicate that almost all inelastic deformations are concentrated within the i^{th} region and that soft-story failure would have likely occurred.

$$R_{1,i} = \frac{\delta_{max,i,U} - \delta_{y,i,U} - (\delta_{max,i,L} - \delta_{y,i,L})}{\delta_{max,roof} - \delta_{y,roof}} \quad (1)$$

2.2 Changes in deformation profile shape

A limitation with $R_{1,i}$ is that if only 3 sensors are used, and the middle sensor is located on the level just below the roof, then it is likely that deformation would be concentrated between the base and middle sensor regardless of deformation type. An alternative feature could be to evaluate changes in the deformation profile shape. For example, elastic and inelastic deformation profile shapes may be more similar in sidesway cases compared to soft-story cases.

The yield and inelastic deformation profile shapes could be estimated by normalizing the corresponding displacement types for a given sensor by those at the roof level. The inelastic deformation profile shape could then be normalized by the yield deformation profile shape to obtain the second potential feature, $R_{2,i}$, shown in Eq (2). If $R_{2,i}$ is close to 1.0, this indicates that the yield and inelastic deformation profile shapes are similar, and that the deformation profile was most likely sidesway.

$$R_{2,i} = \frac{\delta_{y,roof} \cdot (\delta_{max,i,U} - \delta_{y,i,U})}{\delta_{y,i,U} \cdot (\delta_{max,roof} - \delta_{y,roof})} \quad (2)$$

2.3 Consideration of unloaded deformation

$R_{1,i}$ and $R_{2,i}$ were based on the peak response relative to yield deformation. However, the deformation shape after elastic unloading may also be useful. Consider the conceptual soft-story example in Fig. 5. Fig. 5a shows the deformation profile corresponding to (i) yielding, (ii) maximum response, and (iii) elastic unloaded response. The corresponding locations along the hysteretic curve are shown in Fig. 5b.

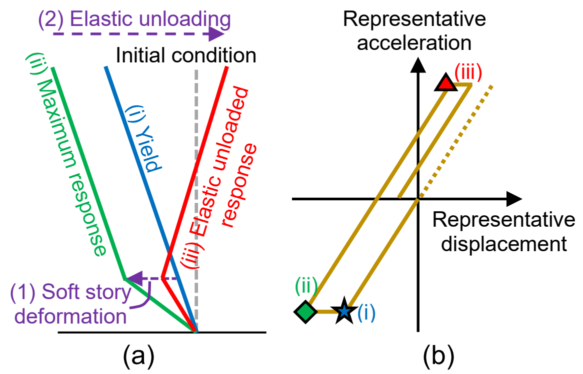

Fig. 5 Elastic unloading after soft-story formation; (a) influence on deformation shape, and (b) respective locations on hysteretic curve

When soft-story occurs, inelastic response concentrates within the soft-story region. This inelastic deformation remains during elastic unloading which may cause the deformation profile to drastically change between the peak and elastically unloaded response. If yielding occurs in the opposite direction, some of the inelastic deformation will be recovered which causes the difference between the deformation profile shapes to decrease. As such, it is better to consider the response just before yielding occurs in the opposite direction (point (iii) in Fig. 5b). If yielding does not occur in the opposite direction, the largest response recorded when unloading can be considered instead.

Based on this concept, the third feature could be based on the ratio of the maximum response shape to that of displacements recovered during elastic unloading (i.e., displacement between points (iii) and (ii) in Fig. 5b). Denoting δ_{unl} as the displacements at point (iii), the third feature can be calculated as:

$$R_{3,i} = \frac{\delta_{max,i,U} \cdot (\delta_{unl,roof} - \delta_{max,roof})}{\delta_{max,roof} \cdot (\delta_{unl,i,U} - \delta_{max,i,U})} \quad (3)$$

3. EVALUATION USING EXPERIMENTAL DATA

3.1 Experimental study details

Shake-table tests of small-scale 5-story steel frames with a single-bay of 1.0 m width were performed to obtain response data for different deformation modes. Four specimen configurations were considered are as follows:

1. TY – total yielding (side-sway) mechanism
2. 1FWS – 1st floor weak story
3. 3FWS – 3rd floor weak story
4. 3FFWS – 3rd floor flexible and weak story

All specimens have interstory heights of 0.36 m. The exception to this was the 3FFWS model, where the 3F-4F story height was increased to 0.50 m so that the the 3rd floor was more flexible compared to the 3FWS model, which results in the elastic deformation shape also exhibiting soft-story deformation tendencies. Photos showing an example of the final deformation recorded for each of the specimen configurations are shown in Photo 1.

All steel members have a cross-section width of 190 mm and thickness of 6 mm. The section width was reduced in locations where inelastic deformation was desired. For the TY configuration, reduced sections were used at the base of the 1F columns and at both ends of all beams. For other configurations, reduced sections were used at the top and bottom of columns within the critical floor. The reduced frame member widths are shown in Table 1. Additionally, steel blocks with dimensions of 110 mm by 110 mm by 150 mm, where the long-dimension is in the out-of-plane direction, was used for masses.

Table 1. Reduced frame member widths

Model	Member	Reduced width (mm)
TY	RF beam	30
	5F beam	50
	4F beam	70
	3F beam	80
	2F beam	70
	1F-2F column	80 (base only)
1FWS	1F-2F column	36
3FWS	3F-4F column	30
3FFWS	3F-4F column	50

Three specimens were assembled for each configuration, with each subjected to a different seismic excitation sequence. Three records were used: (i) an artificial record (WG60), (ii) the east-west component of the 2011 Canterbury Earthquake recorded at Resthaven station (REHS) [4], and (iii) the north-south component of the 1999 Chi-Chi earthquake recorded at station TCU074 station (NGA1509) [5]. Further details of these records were provided in Yeow and Kusunoki [6]. Each record was continuously applied from an initial scale factor of 0.2 and increasing in steps of 0.2 until excessive deformation was observed. For the remainder of this paper, "sequence" will refer to the entire excitation sequence (i.e., from 0.2 scale factor until excessive deformation was reached) while "event" will refer to a single applied excitation (e.g., only the 0.2 scale factor excitation).

The total displacement response of the frame was obtained by applying motion tracking to recorded video footage. The total displacement response of the base was then subtracted from all upper floors to obtain the displacement response of each floor relative to the base. While data were also obtained from strain gauges and accelerometers, these were not considered in this paper. The δ_y, δ_{max} and δ_{unl} values from applying the largest excitation in the WG60 sequence is shown in Fig. 6.

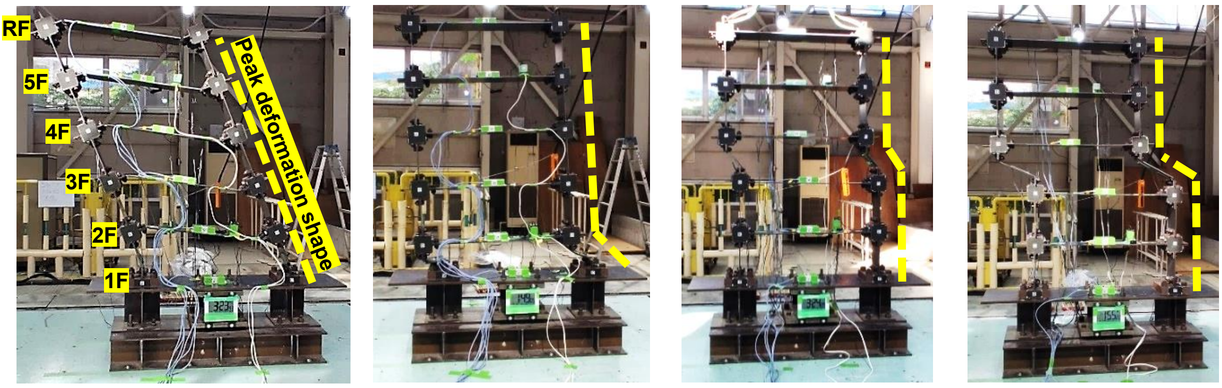

TY 1FWS 3FWS 3FFWS

Photo 1. Final deformation of test specimens (dashed lines show deformation shape)

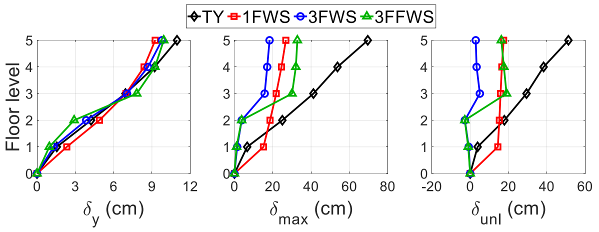

Fig. 6 Displacements from largest excitation in the WG60 sequence for steel experimental models

3.2 Evaluation of features using experimental data

Equations (1)-(3) were applied to results from each excitation of the WG60 sequence to evaluate their suitability for identifying deformation mechanisms. These results are shown in Figs. 7-9 for $R_{1,1}$, $R_{2,1}$ and $R_{3,1}$, respectively. Other sequences had similar trends and are not shown. Here, the ductility response was the maximum representative displacement obtained from each excitation divided by the yield representative displacement estimated by fitting a bilinear curve to the extracted capacity curve considering the entire sequence. Events with ductility less than 1.0 were excluded. It was assumed that only three sensors were used. The middle sensor location was varied between 2F and 5F, while the other two were fixed at 1F and RF.

From Fig. 7, $R_{1,1}$ for soft-story cases (1FWS, 3FWS and 3FFWS) tended to be greater compared to the sidesway case (TY) when the middle sensor was located above the soft-story. Conversely, $R_{1,1}$ was lower when the middle sensor was located below the location of soft-story (e.g., 3FWS and 3FFWS in Figs. 7a-b).

$R_{2,1}$ and $R_{3,1}$ had similar trends where the feature values for soft-story cases tended to be greater than that for the sidesway case when the sensor was located above the soft-story, while the opposite is true when the sensor was located below the soft story. However, in Figs. 8c and 8d, the separation between 1FWS/3FWS and TY was less clear due to relatively small changes in the deformation profile shapes on upper floors between inelastic and elastic response. These results have two implications: (i) $R_{2,1}$ may not work as well as intended and could possibly be discarded as a potential feature, and (ii) it is better to install the middle sensor on a lower floor compared to an upper floor.

The separation between cases for $R_{3,1}$ was less clear at low ductility values as shown in Fig. 9. At greater ductility response, the separation on upper floors is the clearest, indicating that $R_{3,1}$ could be the best to use for such cases.

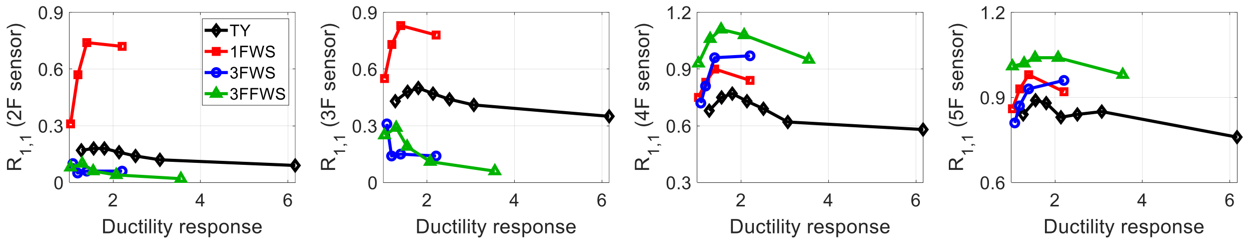

(a) (b) (c) (d)

Fig. 7 Evaluation of $R_{1,1}$ against experimental data for WG60 excitation sequence with middle sensor located on (a) 2F, (b) 3F, (c) 4F and (d) 5F

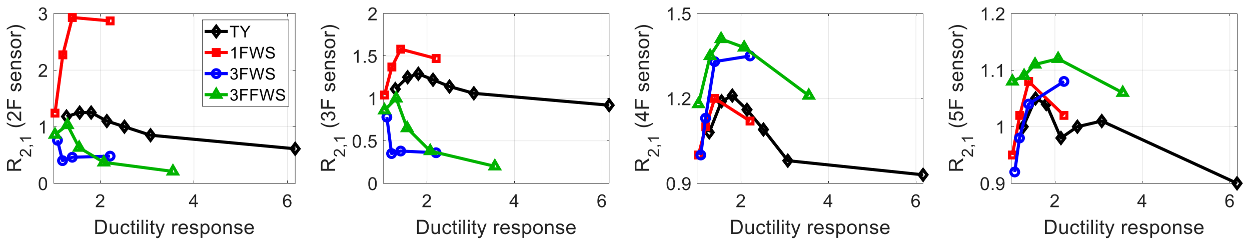

(a) (b) (c) (d)

Fig. 8 Evaluation of $R_{2,1}$ against experimental data for WG60 excitation sequence with middle sensor located on (a) 2F, (b) 3F, (c) 4F and (d) 5F

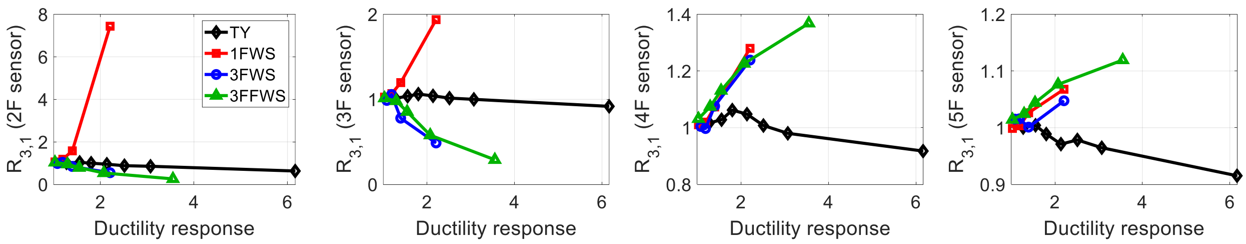

(a) (b) (c) (d)

Fig. 9 Evaluation of $R_{3,1}$ against experimental data for WG60 excitation sequence with middle sensor located on (a) 2F, (b) 3F, (c) 4F and (d) 5F

It should be noted that due to how the feature values change with ductility response, ductility itself should also be considered as a potential feature.

4. EVALUATION USING NUMERICAL STUDY

4.1 Numerical analysis details

The potential features discussed previously were evaluated based on the response of steel frame buildings. To ensure that it is also applicable to RC frame buildings, numerical simulations of RC frames exhibiting different failure modes were performed.

Firstly, numerical models of the steel test specimens were created on OpenSees [6] to ensure accuracy of the analyses. Beam and column elements where yielding was expected to occur was modelled using "beamWithHinges" elements, while others were modelled using "elasticBeamColumn" elements. The "Steel01" (bilinear inelastic) material was used to model the inelastic behavior. The RF relative displacement response of the 1FWS model subjected to the 100% scale event of the WG60 excitation sequence is shown in Fig. 10 for both the analytical and experimental results, where the response was similar.

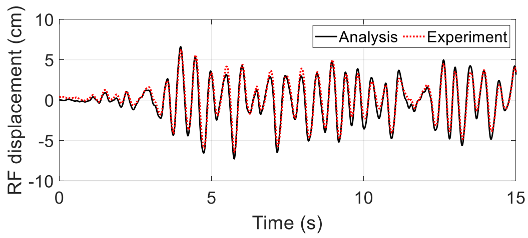

Fig. 10 Comparison of numerical and experimental data (1FWS model, WG60 record, 100% scaling)

To consider RC cases, the hysteresis model was swapped to the "Hysteretic" material to mimic Takeda hysteretic response with an unloading coefficient of 0.4. The WG60 excitation sequence and model names used for the experimental specimens were reused for the numerical modelling of RC buildings. A comparison of the hysteretic materials is shown in Fig. 11.

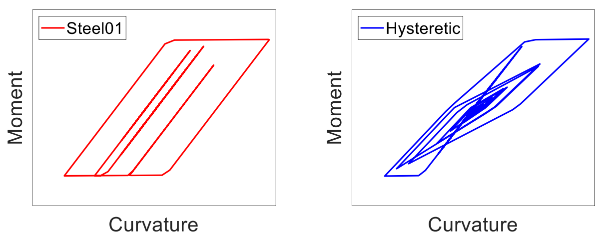

Fig. 11 Adopted hysteresis materials

The δ_y, δ_{max} and δ_{unl} values from applying the largest excitation in the WG60 sequence to the RC models are shown in Fig. 12. The models underwent a smaller ductility response compared to the steel members, resulting in a smaller δ_{max} value. This is because the unloading stiffness of the Hysteretic material is lower than that for Steel01 (from Fig. 10) resulting in lesser accumulation of residual and inelastic deformations. This resulted in the unloaded deformation not exhibiting much soft-story behavior due to lesser residual deformation on the critical floor compared to the steel frames in Fig. 6.

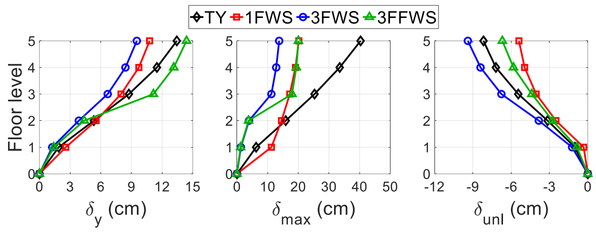

Fig. 12 Displacements from largest excitation in the WG60 sequence for RC numerical models

4.2 Evaluation of features using analytical data

The feature values obtained from numerical analysis results for the WG60 sequence are shown in Figs. 13-15 for $R_{1,1}$, $R_{2,1}$ and $R_{3,1}$, respectively.

The overall trends of the feature values are similar to that observed for the experimental results of steel frames from Figs. 7-9, where the values for the soft-story cases (1FWS, 3FWS and 3FFWS) were typically greater than that for the sidesway case (TY) when using readings of sensors located above the location of soft-story. The opposite is true when considering sensors located below the soft-story location. However, there were instances at low ductility response where the values did not follow the trends, indicating that the features may work better for cases with greater inelastic response where soft-story response was more obvious.

5. CONCLUSION AND FUTURE WORK

Three potential features for identifying the deformation mode of buildings were proposed in this paper. These were based on: (i) the degree of inelastic response, (ii) changes to deformation profile shape, and (iii) unloading deformation profile shape. The suitability of the features were evaluated against experimental and analytical data. While it was shown that all three features have potential to identify soft-story failure, the identification was clearer when greater inelastic response occurred. Therefore, ductility response should also be included as a suitable feature.

The next step for identifying the deformation mode would be to develop a classifier machine learning model based on the proposed features using a larger building response database. This should contain a wider range of building properties (e.g., stiffness, strength, ductility capacity), ground motions, and failure modes. The suitability of features based on other response measures, such as acceleration and/or velocity response, should also be evaluated.

ACKNOWLEDGEMENT

The first author is an overseas researcher under the Postdoctoral Fellowship of Japan Society for the Promotion of Science (JSPS), and the present work is supported by the Grant-in-Aid for JSPS Fellows.

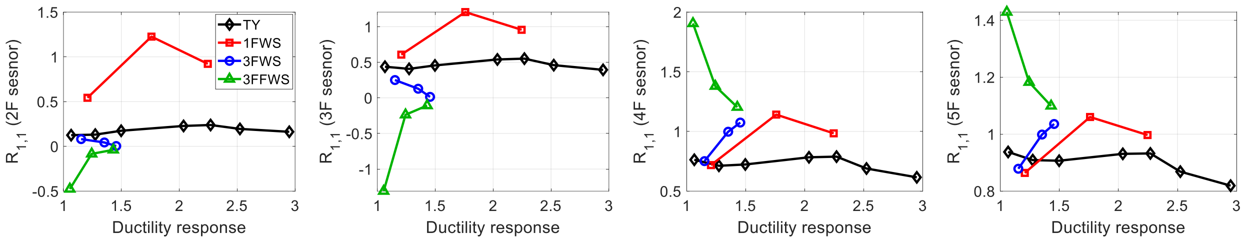

(a) (b) (c) (d)

Fig. 13 Evaluation of $R_{1,1}$ against numerical results for WG60 excitation sequence with middle sensor located on (a) 2F, (b) 3F, (c) 4F and (d) 5F

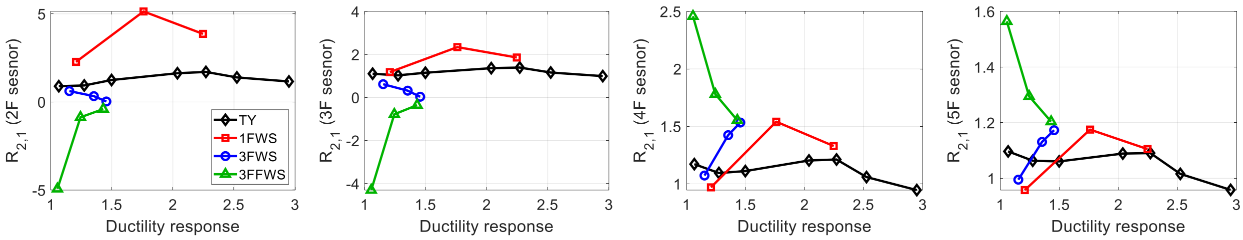

(a) (b) (c) (d)

Fig. 14 Evaluation of $R_{2,1}$ against numerical results for WG60 excitation sequence with middle sensor located on (a) 2F, (b) 3F, (c) 4F and (d) 5F

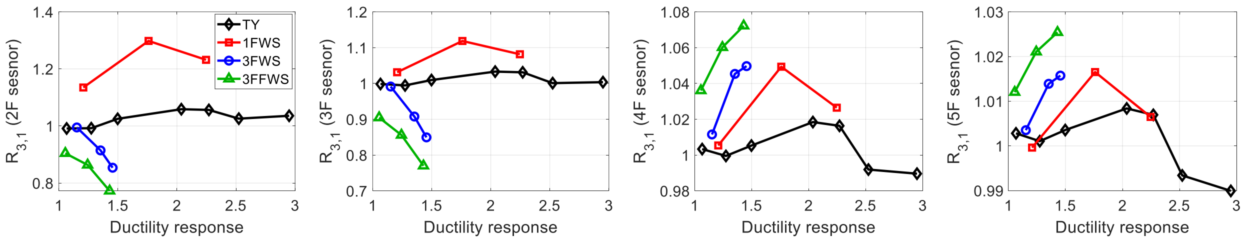

(a) (b) (c) (d)

Fig. 15 Evaluation of $R_{3,1}$ against numerical results for WG60 excitation sequence with middle sensor located on (a) 2F, (b) 3F, (c) 4F and (d) 5F

REFERENCES

[1] Kusunoki, K., Hinata, D., Hattori, Y., and Tasai, A. "A new method for evaluating the real-time residual seismic capacity of existing structures using accelerometers: structures with multiple degrees of freedom", Japan Architectural Review, Vol 1(1), pp 77-86, 2018.

[2] Kusunoki, K. "Experimental study on the damage classification method with the performance curves of R/C structures derived from recorded accelerations", Journal of Structural and Construction Engineering, Vol. 85(744), pp 1055-1065, 2020. (in Japanese)

[3] Chen, C., and Kusunoki, K. "consideration on capacity curve of buildings with a few acceleration sensors", Summaries of Technical Papers of Annual Meeting, Architectural Institute of Japan, pp 343-344, 2022. (in Japanese)

[4] Bradley, B. A., and Cubrinovski, M. "Near-source strong ground motions observed in the 22 February 2011 Christchurch Earthquake", Seismological Research Letters, 82(6), pp 853-865, 2011.

[5] Chiou, B. S. J., Darragh, R., Gregor, N., and Silva, W. "NGA project strong-motion database", Earthquake Spectra, 24(1), pp 23-44, 2008.

[6] Yeow, T. Z., and Kusunoki, K. "Shake-table test of eccentrically-loaded steel frames" Summaries of Technical Papers of Annual Meeting, Architectural Institute of Japan, pp 205-206, 2022.

[7] McKenna, F., Fenves, G. L., and Scott, M. H. "Open system for earthquake engineering simulation (OpenSees)", University of California, Berkeley, 2000.